Science of Sintering, **50** (2018) 255-273

doi:https://doi.org/10.2298/SOS1802255K

UDK 547.458.2; 665.587

Influence of Temperature and Different Hydroxides on Properties of Activated Carbon Prepared From Saccharose. Characterization, Thermal Degradation Kinetic and Dyes Removal From Water Solutions

Sanja S. Krstić[1], Milan M. Kragović[1*)], Vladimir M. Dodevski[1], Aleksandar D. Marinković[2], Branka V. Kaluđerović[1], Gregor Žerjav[3], Albin Pintar[3], Maja C. Pagnacco[4], Marija D. Stojmenović[1]

[1]University of Belgrade, Vinča Institute of Nuclear Sciences, Mike Petrovića–Alasa 12–14, P.O. Box 522, Belgrade, Serbia

[2]University of Belgrade, Faculty of Technology and Metallurgy, Karnegijeva 4, P.O.B, 3503, 11001 Belgrade, Serbia

[3]Department for Environmental Sciences and Engineering, National Institute of Chemistry, Hajdrihova 19, SI-1001 Ljubljana, Slovenia

[4] Faculty of Physical Chemistry, University of Belgrade, Studentski trg 12-16, 11000 Belgrade, Serbia

Abstract:

In presented paper, influence of temperature, precursor concentration and different hydroxides on properties of activated carbon obtained from saccharose were investigated. The samples were prepared by hydrothermal treatment and activated using KOH, NaOH and LiOH. Two saccharose concentrations (0.5, 1.0 mol/dm^3) and three temperatures (160, 200, 240 ºC) were changed in hydrothermal treatment. Activation processes were performed at 750 ºC under N_2 atmosphere. Samples were characterized by X-ray powder diffractometry, elemental analysis, N_2 adsorption-desorption measurements, Fourier-transform infrared spectrometry, scanning electron microscopy and thermal analysis. The obtained samples were tested for potential application in dyes removal from water solutions.

Keywords: *Saccharose; Activated carbon; Hydrothermal treatment; The energy source; Dye removal.*

1. Introduction

In recent years, a great number of research papers have been published regarding hydrothermal synthesis of functional and novel carbonaceous materials with size-controlled particles. The topic is very intriguing due to variety of applications of carbonaceous materials such as: adsorbents [1], filter materials [2], catalysts [3-5], nano devices [6], energy storage [7, 8], drug delivery [9, 10], separation technology [11, 12], *etc*. Activated carbons may be prepared in different forms. Morphology of these materials and their properties such as thermal isolation, low weight and high compressive strength attracted a significant attention

*) **Corresponding author:** m.kragovic@vin.bg.ac.rs

in the world of carbon materials. Black solid carbons obtained by hydrothermal synthesis contain carbon microspheres during thermos-destruction of organic compounds under conditions of oxygen deficiency, not only the release of CO and CO_2, but also occurs formation of carbon [13]. Recently activated carbon microspheres have attained popularity because of their advanced properties in comparison with carbon monoliths [13], carbon fibres [14] and granular form of activated carbon materials [15] or active carbon powders [16]. Spherical form of carbon materials pose better adsorption capacity, smooth surface, good packaging property, reduced ash content, low-pressure drop, good mechanical strength, high micropore volume and controllable pore size distribution [17].

Owing to all these properties, activated carbon microspheres are becoming very important and usable in different fields of applications.

A variety of methods have been developed to prepare carbon materials with different properties. Applying hydrothermal synthesis, carbon microspheres obtained in aqueous solution from different carbohydrate precursors were formed in solid state containing micro- and nano-particles of different size, shape and carbon content. For formation of carbon microspheres, saccharides, such as glucose, starch, saccharose and cellulose were used in dehydration process [18]. The obtained microspheres have characteristic morphology, chemical structure and surface properties, and they can be widely used in environmental applications and medicine [19]. Bearing in mind economic and environmental aspects, hydrothermal carbonization of carbohydrates belongs to a new trend of the green route of the synthesis of material with potential applicability and comparative properties/advantages.

One of the most used precursor material for carbon microspheres synthesis is saccharose. The formation of carbon microspheres by hydrothermal treatment of saccharose takes place through processes of dehydration, condensation or polymerization and aromatization reactions [20]. Particles obtained from saccharose as precursor were spherical with size in the range from 0.3 to 10 μm, whereas those synthesized from glucose were in the range from 250 to 550 nm [21]. Generally, the synthesis process consists aromatization process under hydrothermal conditions, with spherical carbon containing highly aromatic nucleus and a hydrophilic shell [18, 22] Many factors of synthesis affect the yield, morphology and surface functional groups of spherical carbon materials obtained from saccharose as precursor. The diameter of these carbon microspheres can be controlled by modifying synthesis conditions. It was shown that increase of the reaction temperature, saccharide concentration or reaction time leads to a changed diameter [21]. In general, one of the most important application of activated carbon is in removal of different pollutants (organic, such as dyes, or inorganic like heavy metals) from environment. This application is especially interesting when activated carbon is obtained from easy available, low-cost and eco-friendly materials such as saccharose.

Wide use of dyes by multifarious industries causes intense and constant damage to the environment because of their high toxicity and non-biodegradability [23]. It is difficult to conduct degradation of dye materials because they are very sTab. against light and oxidation reactions [24]. Adsorption and removal of dyes from wastewaters before further discharge in environment is a necessary step for the water industry and environmental safety. Methylene blue (MB), basic cationic dye is one of the most common dying materials for wood, cotton, silk and other textiles [25]. Also, methyl orange (MO) is acidic/anionic dye, and has its application as in textile, printing, paper, food and pharmaceutical industries, in research laboratories too [26]. Uniform or long exposure to MO or MB can cause many health problems such as increased heart rate, cyanosis, jaundice, vomiting, shock, quadriplegia, and tissue necrosis in human organisms [27]. For that reason, removal of MO and MB from wastewaters and industrial discharges is very important because of their potential toxicity to humans and the environment. Because of their harmful properties, MO and MB were selected as the model dyes in this paper. In previous investigations, various adsorbents such as iron

terephthalate (MOF-235) or magnetic cellulose beads entrapping activated carbons have been applied by other authors [28, 29] for the removal of both MO and MB dyes.

The aim of the present paper is to investigate the influence of process parameters (concentration of precursor and treatment temperature) on the properties of samples obtained by hydrothermal carbonization, as well as on the properties of samples activated by different hydroxides. The obtained samples were characterized in detail. Since, thermal pyrolysis provides a sustainable way for recycling organic materials and offers possibility of transforming organics into fuel it was of interest to investigate thermal degradation kinetic of the samples and their potential application as a source of energy. Application in field of environmental protection was investigated on adsorption of dyes from contaminated water solutions.

2. Experimental

2.1. Synthesis of activated carbon materials

Synthesis of activated carbon materials was performed in two steps: the first step was hydrothermal synthesis of carbon containing material which was used further for hydroxide activation as second step.

At first, required amount of saccharose (S) was dissolved in the deionized water and two saccharose solutions with different concentrations (0.5 and 1.0 mol/dm^3) were prepared. Hydrothermal synthesis of carbon microspheres was carried out in the PTFE (polytetrafluoroethylene) chamber placed in stainless steel autoclave. Prepared solutions were placed into autoclave and heated in a oven under autogenous pressure at 160, 200 and 240 °C for 24 h. Afterwards, prepared samples were filtrated, washed with distilled water and dried for 1 h at 100 °C.

The second part of this experiment was activation of the carbon containing material with microsphere structure with selected hydroxides (KOH, NaOH and LiOH) as activation agents. Activation was performed by dry physical mixing of selected microsphere precursor and hydroxide at room temperature with the ratio 1:3 (Tab. I).

Subsequently, the mixed samples were activated in a horizontal tube furnace (Protherm Furnaces, model PTF 16/38/250, Turkey) at 750 °C, 200 cm^3/min of nitrogen flow and the heating rate of 5 °C/min, with retention time of 1 h.

The obtained microspherical carbons were denoted as HTC@S–T–M–t before activation, where: S is precursor, T is temperature of HTC treatment, M is solution molarity and t is HTC treatment time. Sample after process carbonization was designated as C@S–T–N_2–t, where: S is precursor, T is carbonization, N_2 is activation gas and t is carbonization time. After activation, activated carbons were denoted as AC@S–T–N_2–t–XOH, where: S is precursor, T is activation temperature, N_2 is activation gas and t is activation time and XOH activation agents.

2.2. Characterization methods

In order to investigate phase composition and structural arrangement of investigated samples, X-ray powder diffraction (XRPD) method was used. Ultima IV Rigaku diffractometer, was equipped with Cu$K_{\alpha 1,2}$ radiation, a generator voltage (40.0 kV) and a generator current (40.0 mA). The range of 10–90° 2θ was used for all powders in a continuous scan mode with a scanning step size of 0.02° and at a scan rate of 5 °/min. All powders were compared using ICDD data base [30].

Morphology of samples was investigated by a scanning electron microscope (SEM) JEOL JSM–5800. The sphere diameters were determined applying Image Pro Design program and results were presented in form of histograms.

Textural characteristics of activated carbons were determined by measuring nitrogen adsorption−desorption isotherms at −196 °C using a Micromeritics (model TriStar II 3020). Before measurement, the samples were degassed under a nitrogen stream (purity 6.0) and programmed bi–level heating, starting with the first heating stage at 90 °C for 60 min and followed by the second heating stage at 250 °C for 240 min. According to the recommendations for carbon materials [31], specific surface area (S_{BET}) was calculated by means of BET (Brunauer, Emmet, Teller) equation from the best linear fit in the region $p/p^o < 0.01$ (p and p^o represent the equilibrium and saturation pressures of nitrogen at fixed temperature). Besides S_{BET}, the pore size distribution, mesopore surface (S_{meso}) and micropore volume (V_{micro}) were also calculated from the isotherms. Pore size distribution was calculated from the desorption branch of the nitrogen isotherm, employing the BJH (Barrett, Joyner and Halenda) method (Barrett et al. 1951). Mesopore surface area and micropore volume were estimated using the high resolution α_s–plot method [32-35]. Micropore surface was calculated by subtracting mesopore surface from the specific surface area.

Fourier-transform infrared (FTIR) spectra of the investigated active carbons were collected using a Thermo Fisher Scientific FTIR spectrometer IS-50, in the transmission mode. The samples were prepared by using pressed KBr pellets (0.2 mg of the sample: 80 mg KBr) technique. The spectra were recorded in the range from 4000 to 400 cm^{-1} with 64 scans and resolution of 2 cm^{-1}. After recording of the spectra, two corrections were performed: automatic correction of the base line and atmospheric suppression.

Thermal analysis (thermogravimetric (TGA) and differential thermal analysis (DTA)) of investigated samples were performed on a Netzsch STA 409 EP. Samples were heated from 25 to 1000 ^oC in an air atmosphere at the heating rate of 10 ^oC/min. Thermal degradation kinetic was also followed on the same instrument by heating samples from 25 to 1000 ^oC in an air atmosphere at heating rates of 5, 10, 15 and 20 ^oC/min. Prior to analysis, samples were kept in a desiccator at a relative humidity of 23 %.

2.3. Adsorption experiments

The adsorption experiments for dyes were carried out in magnetically stirred (σ = 400 rpm) glass vessel. All measurements were performed with the same concentration (50 mg/dm^3) of MB and MO at initial pH value 6.6, at room temperature (T= 23 ^oC) and under conditions protected from light. The solid/liquid ratio applied in these experiments was 25 mg/25 cm^3. At a specific time, the samples were taken, centrifuged and analyzed on Agilent 8435 UV–VIS spectrophotometer with diode array detector. The absorption spectra of dye solutions were collected after certain reaction time intervals and at the certain absorption wavelength, λ_{max}= 665 nm for MB, and λ_{max}=466 nm for MO, as well.

3. Results and discussion

3.1. XRPD analysis

XRPD patterns of all samples are presented at Fig. 1 and 2. The XRPD analysis of samples HTC@S–T–M (Fig. 1a-f) and C@S–T–N_2–t (Fig. 2a) shows a broad peak between 10 and 20° of the 2θ value, which is characteristic for carbonaceous materials [36]. In addition, the XRPD analysis illustrates that samples of active carbons AC@S–750–N_2–1.0–KOH (Fig. 2b), AC@S–750–N_2–1.0–NaOH (Fig. 2c) and were clearly formed in an amorphous state. This was corroborated by the occurrence of two peaks positioned at around 2θ=26º and 2θ=44º, which are ascribed to typical graphitic (002) and (100) planes. In contrast to these results, XRPD pattern of sample AC@S–750–N_2–1.0–LiOH (Fig. 2d) shows sharp and well defined peaks indicating that this material has a defined structural arrangement. According to these results, it can be assumed that applying the presented method of

hydrothermal carbonization, the pure nano Li_2CO_3 material (ICDD 01–074–6256) [30] can be synthesized in the form of a deposit on the surface of microsphere precursor. Therefore, it was necessary to perform additional XRPD analysis on carbonate content after carbonization in air at 600 °C (Fig. 2e). After carbonization process and additional XRPD analysis, the dominant presence of Li_2O (ICDD 01-072-1216) [30] was determined, which is in agreement with the results of elemental chemical composition (Tab. I).

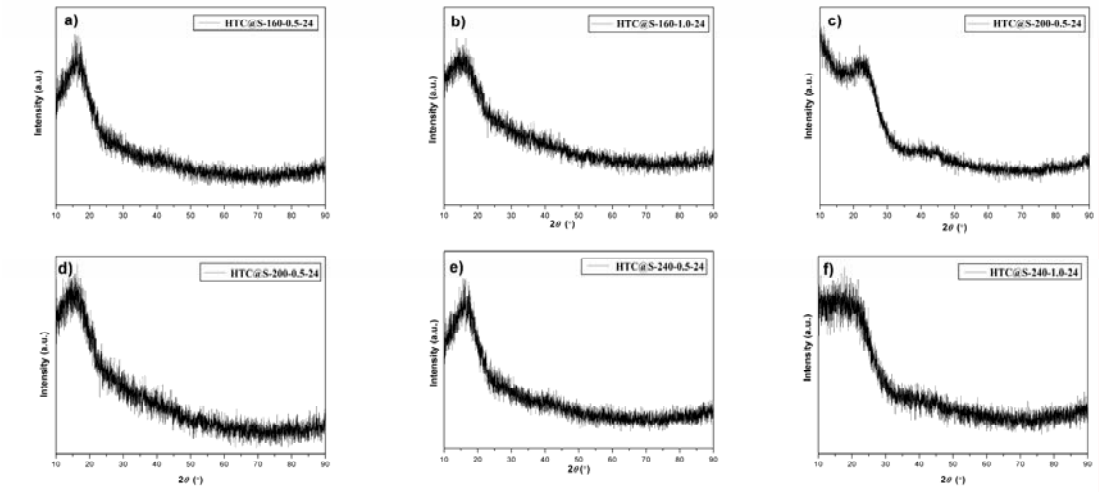

Fig. 1. XRPD analysis of (HTC@S–T–M–t)

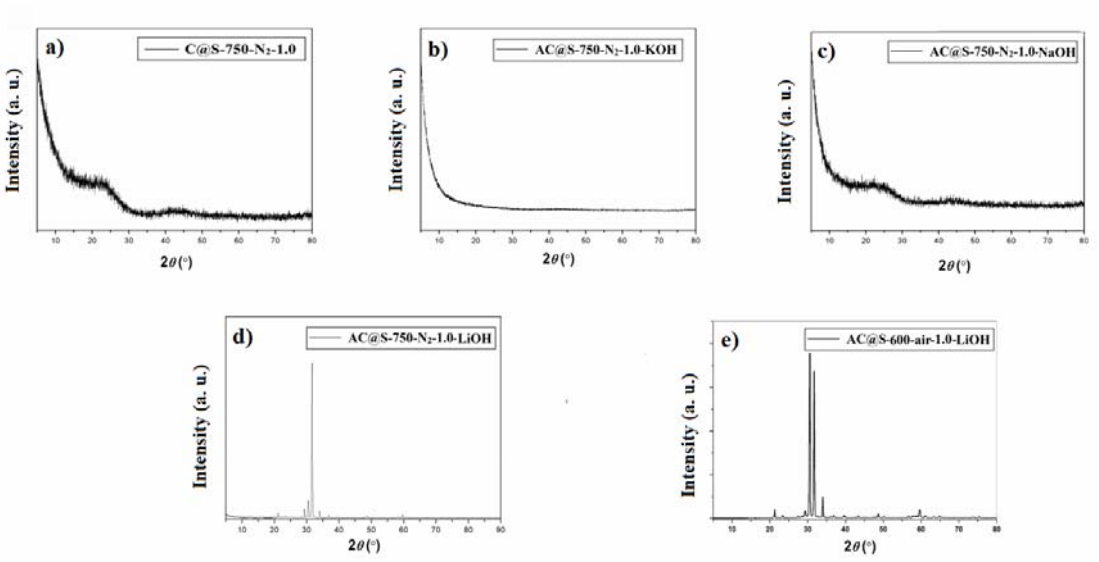

Fig. 2. XRPD analysis of(C@S–T–N_2–t) and (AC@S–T–N_2–t–XOH).

3.2. Elemental analysis

The elemental chemical composition (C, N, O and H) of investigated samples are listed in Tab. I. It can be noted that with increase of HTC treatment temperature, the content of carbon is increased from 42.1 % in raw saccharose to approximately 70 % in carbon microspheres HTC@S–T–M–t obtained by hydrothermal treatment of saccharose. Further, after carbonization process the content of carbon in C@S–T–N_2–t increased to ~87 %. After activation process, only AC@S–750–N_2–1.0–NaOH retained the same content of carbon (~87 %). The content of carbon in AC@S–750–N_2–1.0–KOH was slightly lower (83.6 %), while

the content of carbon in AC@S–750–N_2–1.0–LiOH significantly decreased to 36.6 %. The significant difference in percentage of carbon content in AC@S–750–N_2–1.0–LiOH in comparison with samples activated with KOH and NaOH can be explained by presence of the crystal phase with composition of Li_2CO_3 [30] or Li_2O. That is proved by with XRPD analysis (Fig. 2e) (ICDD 01-072-1216) [30] of thermal treated sample activated with LiOH in an air atmosphere at 600 °C, where is determined presence of Li_2O in percentage of 63.4 %.

Tab. I Elemental analysis of raw saccharose, carbon microspheres obtained by hydrothermal treatment (HTC@S–T–M–t), carbon microspheres after carbonization process (C@S–T–N2–t) and activated carbons with different hydroxides (AC@S–T–N2–t–XOH).

Samples	N (%)	C (%)	H (%)	O (%)	Yield (%)
Raw saccharose	0.023	42.101	6.720	48.844	/
HTC@S–160–0.5–24	0.023	61.558	5.367	33.052	27.2
HTC@S–160–1.0–24	0.063	61.651	5.476	32.810	26.5
HTC@S–200–0.5–-24	0.137	62.998	4.744	32.121	25.7
HTC@S–200–1.0–24	0.128	63.945	4.818	31.108	25.6
HTC@S–240–0.5–24	0.066	69.911	6.133	23.891	25.3
HTC@S–240–1.0–24	0.047	69.925	6.148	23.881	25.3
C@S–750–N_2–1.0	0.261	87.480	2.361	9.898	33.3
AC@S–750–N_2–1.0–LiOH	0.071	36.597	0.637	*	17.2
AC@S–750–N_2–1.0–NaOH	0.491	87.510	5.615	6.384	8.3
AC@S–750–N_2–1.0–KOH	0.087	83.613	5.630	10.670	12.5

3.3. SEM analysis

Influence of temperature and concentration of saccharose as precursor on morphology and microstructure of the synthesized carbon material is shown in Fig. 3. SEM micrographs showed a low degree of dependence of morphology and microstructure of microspheres from temperature and the precursor concentration. Carbon microspheres at 160 and 200 °C (Fig. 3a-d) consist a large amount of uniform microspheres with the diameter range between ~1.0 and ~1.5 μm, which is documented by histograms of diameter distribution (Fig. 5a-d). Carbon microspheres obtained by hydrothermal treatment at 240 °C (Fig. 3e and 3f), are partly agglomerated with diameter range between ~1.1- ~1.4 (Fig. 5e and f).

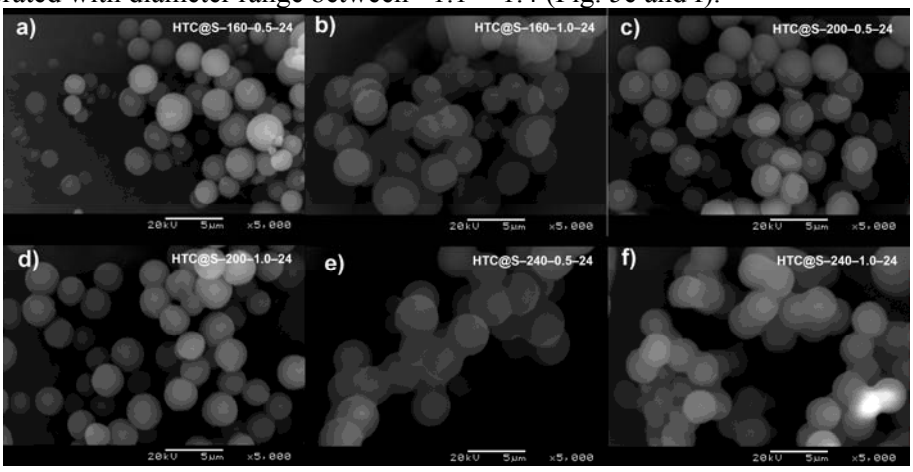

Fig. 3. SEM micrographs of carbon microspheres obtained by hydrothermal treatment of saccharose (HTC@S–T–M–t).

In accordance with the highest content of carbon (69.925 %) and satisfactory yield (25.3 %) after HTC treatment (Tab. I), the sample HTC@S-240-1.0-24 was selected for further investigation. Thus, this sample was subjected to process of carbonization (C@S–750–N_2–1.0) and similar trend was also observed in SEM micrograph (Fig. 4a) with appearance of partly disarranged and agglomerated carbon microspheres. Histogram of diameter distribution shows the presence of some small microspheres with the average diameter of ~1.1 μm (Fig. 5g).

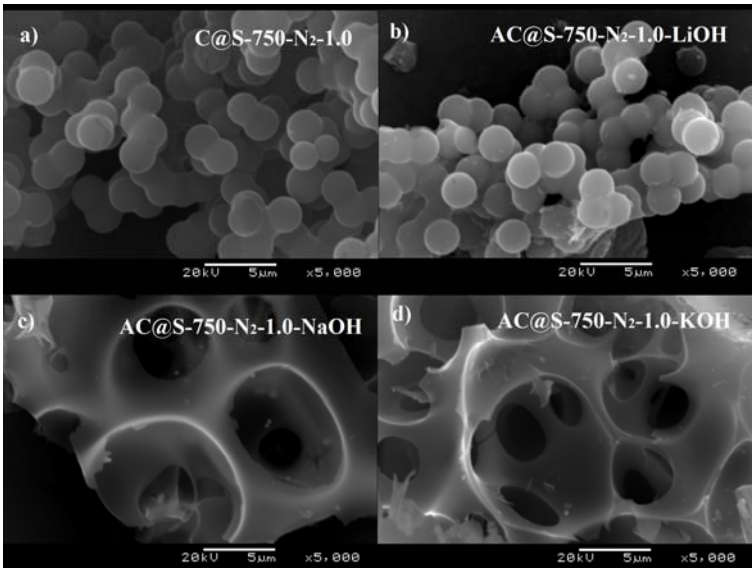

Fig. 4. SEM micrographs of a) (C@S–T–N2–t) and b) (AC@S–T–N_2–t–XOH) (b-d).

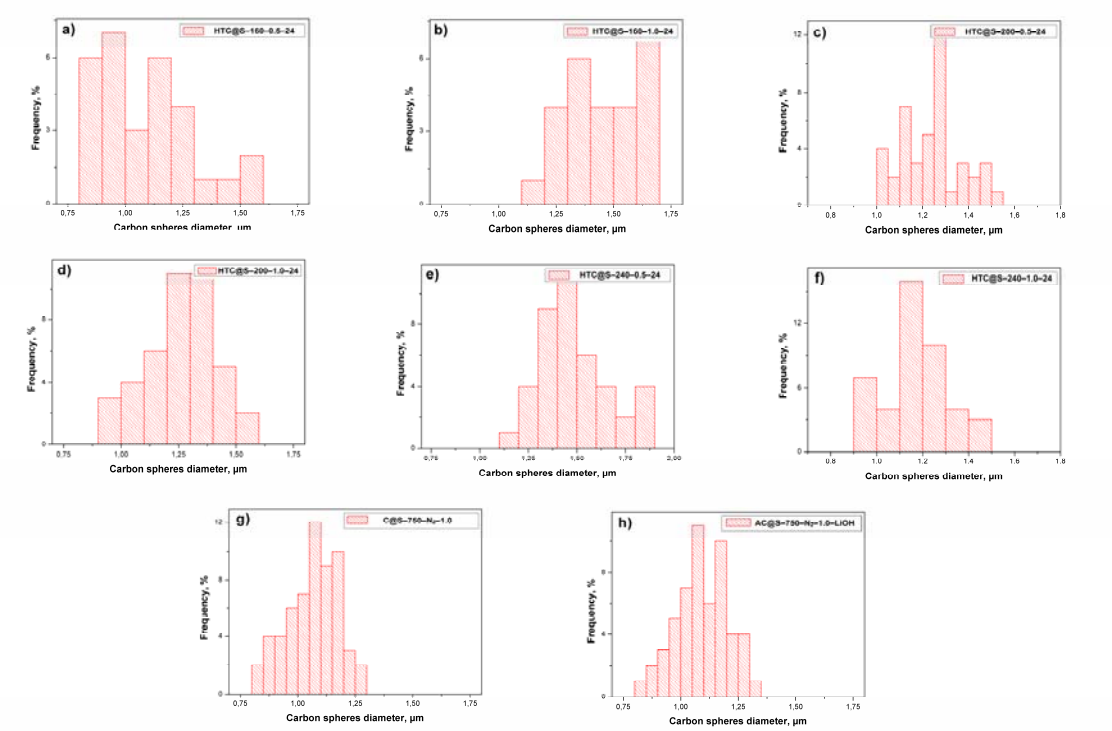

Fig. 5. Histograms of diameter distribution of (HTC@S–T–M–t) (a-f), (C@S–T–N_2–t) (g) and AC@S–750–N_2–1.0–LiOH (h).

Carbon microspheres activated with NaOH and KOH at 750 °C in nitrogen flow (Fig. 4c and d), changed their spherical shape and became disordered. The main reason for these changes may be the result of high precursor/hydroxide ratio (1:3). Contrary to that, carbon microspheres activated with LiOH, partly maintained their microspherical structure (Fig. 4b), and kept the average diameter of ~1.1 μm (Fig. 5h).

With change of reaction temperature and precursor concentration, the degree of agglomeration of particles increased, with relatively low loss in the uniformity in size of particles. The carbon content was not significantly changed with increase of concentration of the precursor, but with increase of the reaction temperature carbon content slightly increased.

3.4. BET analysis

Textural properties of obtained samples were determined by nitrogen adsorption-desorption at –196 °C. Samples HTC@S–T–M–t and C@S–T–N_2–t do not possess good textural properties (S_{BET} <10 m^2g^{-1}) (results are not shown). On the other hand, activated carbon materials (AC@S–T–N_2–t–XOH) demonstrate a significant increase of specific surface area (S_{BET}; Tab. II). The samples of activated carbons AC@S–T–N_2–t–XOH reveal similar isotherm profiles characteristic of type I according to IUPAC classification (Sing et al. 1985) (Fig. 6.) along with uniform mesopore size (Figs. 6b, 6c and 6d). In the Fig. 6., the filled symbols present the adsorption branch, while the empty ones correspond to the desorption branch. Specific surface areas calculated by BET equation (S_{BET}) are listed in Tab. II.

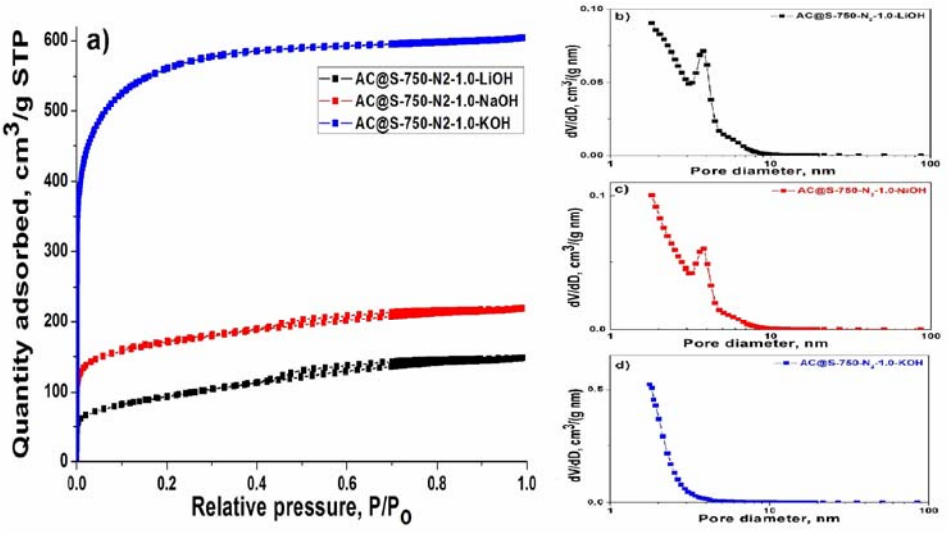

Fig. 6. N_2 adsorption–desorption isotherms of activated carbons obtained by using different hydroxides (AC@S–T–N_2–t–XOH).

Tab. II Textural properties of activated carbons (AC@S–T–N_2–t–XOH). Specific surface areas (S_{BET}), mesopore surface (S_{meso}), micropore surface (S_{mic}), micropore volume (V_{mic}) and average pore width (d_{pore}).

Samples	S_{BET} (m^2g^{-1})	S_{meso} (m^2g^{-1})	S_{mic} (m^2g^{-1})	V_{mic} (cm^3g^{-1})	d_{pore} (nm)
AC@S–750–N_2–1.0–LiOH	323	11	312	0.20	3.0
AC@S–750–N_2–1.0–NaOH	622	14	608	0.16	3.3
AC@S–750–N_2–1.0–KOH	2094	17	2077	0.32	2.3

As it may be seen from Tab. II, after activation with different hydroxides, significant increase of specific surface area occurred and their values were between 323–2094 m^2g^{-1}. With increase of atomic radii of metal ion in hydroxide used, specific surface area increased. Based on the standard nitrogen adsorption isotherms (Fig. 6a) α_s -diagrams have been plotted and mesoporous surface area (S_{meso}) including contribution of external surface and micropore volume (V_{mic}) were calculated. Further, micropore surface (S_{mic}) was determined by subtraction of the S_{meso} from the S_{BET}. All calculated porosity parameters (S_{meso}, S_{mic}, V_{mic}) are also listed in Tab. II. Presented results for samples activated by NaOH and KOH indicate developing of the dominant microporosity with disturbed spherical structure, whereas sample activated by LiOH retain spherical structure.

3.5. FTIR analysis

In order to acquire information on the type of functional groups at the surface of carbon microspheres obtained by hydrothermal treatment of saccharose (HTC@S–T–M–t), carbon microspheres after carbonization process (C@S–T–N_2–t) and activated carbons obtained by using of different hydroxides (AC@S–T–N_2–t–XOH), FTIR spectra were measured and results are illustrated in Fig. 7. The FTIR spectra of AC@S–T–N_2–t–XOH are very similar to the FTIR spectra of HTC@S–T–M–t and C@S–T–N_2–t, with the difference of peaks intensity. The attribution of specific vibrational modes of carbon surface can be very demanding and complicated in the case of carbon microspheres, due to the interaction of functional groups with each other. The formation of carbonaceous spheres by the hydrothermal treatment of different carbohydrate precursor was well described in the literature [18, 21, 37].

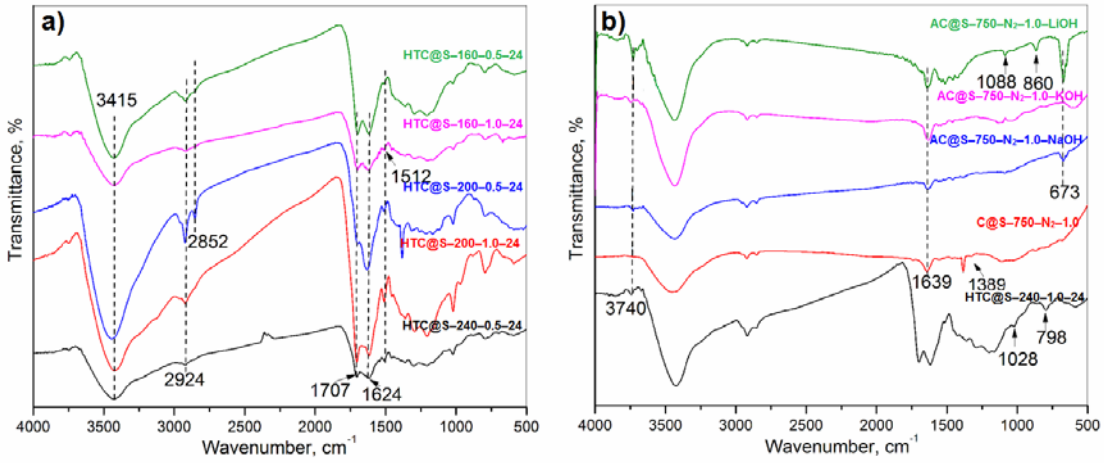

Fig. 7. FTIR analysis of (HTC@S–T–M–t), (C@S–T–N_2–t) and (AC@S–T–N_2–t–XOH).

Processes of formation of the final form of microsphere take place by aggregation of nano–sized primary particles. Generally, process includes three steps: first one consists of conversion of carbohydrate precursor to hydroxymethyl furfural (HMF) *via* intra-molecular dehydration by losing stoichiometric quantity of the water [38]. The HMF molecule is a hydrophilic and water-soluble molecule possessing high reactive potential: hydroxymethyl and aldehyde groups, and two hydrogen atoms at furan ring. It was shown in the literature, according to the Mulliken charge distribution of HMF [39], that three of six terminals are most active and are most likely to participate in different reactions. Considering that HMF is a two–functional reactant, polycondensation reactions could take place under applied hydrothermal condition at two and five positions with release water molecule in the second

step. Polycondensation of HMF causes creation of polymeric chain with 3D network-like structure. In addition, in the third step due to its high reactivity HMF is able to react through different reaction routes: interconversion, tautomerisation and fragmentation/decomposition (*i*.e., ring scission by breaking of C–C bond). It was undoubtedly evidenced that carbonaceous materials are mainly composed of three–dimensional cross–linked furanic rings [40].

It can be seen in this study that the FTIR spectra of the samples obtained after hydrothermally treated saccharose at 160 and 240 °C (HTC@S–T–M–t) are very similar, confirming that there is no special chemical transformation during temperature change. From the spectra (Fig. 7) several characteristic bands can be observed revealing that polycondenzation/aromatization processes take place during hydrothermal carbonization. The presence of unsaturated moieties evidenced by the band at about 1620 cm^{-1}, is attributed to C=C skeletal stretching vibrations [41, 42]. In addition, the bands in the 875–750 cm^{-1} region could be assigned to vinylic C–H out–of–plane bending vibrations. The presence of saturated aliphatic structure was deduced from the band at about 3000–2815 cm^{-1}, which corresponds to stretching, asymmetric and symmetric vibrations of C-H bond. Moreover, the presence of hydroxyl group is suggested by the bands at 3000–3700 cm^{-1}, whereas a broad band is attributed to O–H stretching vibrations in hydroxyl or carboxyl groups. Appearance of band at about 1707 cm^{-1}, which corresponds to carbonyl stretching vibration, indicates the presence of carbonyl group C=O in carboxyl, quinone or ester [42]. Presence of oxygen containing groups is also evidenced by bands in 1000–1460 cm^{-1} region, which could be ascribed to C–OH stretching vibrations in hydroxyl, ester or ether, and O–H bending vibrations [41, 42]. Partially dehydrated residues in which reductive O–H or C–OH groups are covalently bonded to the carbon frameworks improve the hydrophilicity and stability of the microspheres and greatly widen their range of applications. Therefore, a significant amount of oxygen–containing functional groups on the surface of all investigated carbonaceous microspheres, formed by hydrothermal synthesis, makes their surface more hydrophilic and capable for further transformation creating possibility for different applications.

3.6. Thermal analysis

Results of thermal analysis (TGA/DTA) of saccharose, samples after carbonization C@S–750–N_2–1.0 and activation process AC@S–750–N_2–1.0–KOH are shown at Fig. 8. From Fig. 8a it is clear that TGA curve for saccharose shows nonlinear trend, while at DTA curve one endothermic and two exothermic peaks are visible. In the first temperature interval (25–200 °C) the DTA curve of pure saccharose reveal broad endothermic behavior and peak at 190 °C is visible and corresponds to saccharose melting. In the same time, at this temperature interval, due to moisture loss, a weight loss of 2.20 % was observed at TGA curve [43]. At higher temperatures, saccharose decomposes and mass loss of 99.70 % was observed at TGA curve in temperature interval 200–1000 °C. The saccharose decomposition follows equation:

$$C_{12}H_{22}O_{11} \rightarrow 12C+11H_2O \quad (1)$$

This process was followed with two exothermic peaks at DTA curve with maximums at 370 °C (due to carbonization which include formation of polyaromatics and carbon sheets and graphenes) and 505 °C (due to char structure changes) [44,45].

As it may be seen from Fig. 8b (C@S–750–N_2–1.0) the TGA curve showed a nonlinear trend. In the first temperature range (25–200 °C) moisture loss occurred. This process was followed with weight loss of 5.20 % on the TGA curve and with endothermic peak with minimum at 59 °C on the DTA curve. In the second temperature region (200–1000 °C) decomposition of the organic components in the investigated sample occurred and this process has been finished at ~800 °C. Further increase of the temperature up to 1000 °C did

not lead to significant changes on the TGA curve and total weight loss of about 86 % was detected for the temperature range between 200 and 1000 °C. Decomposition of the organic phase in the sample was also followed with two exothermic peaks on the DTA curve which maximums were shifted towards higher temperatures in comparison to saccharose and due to modification observed at 475 and 702 °C.

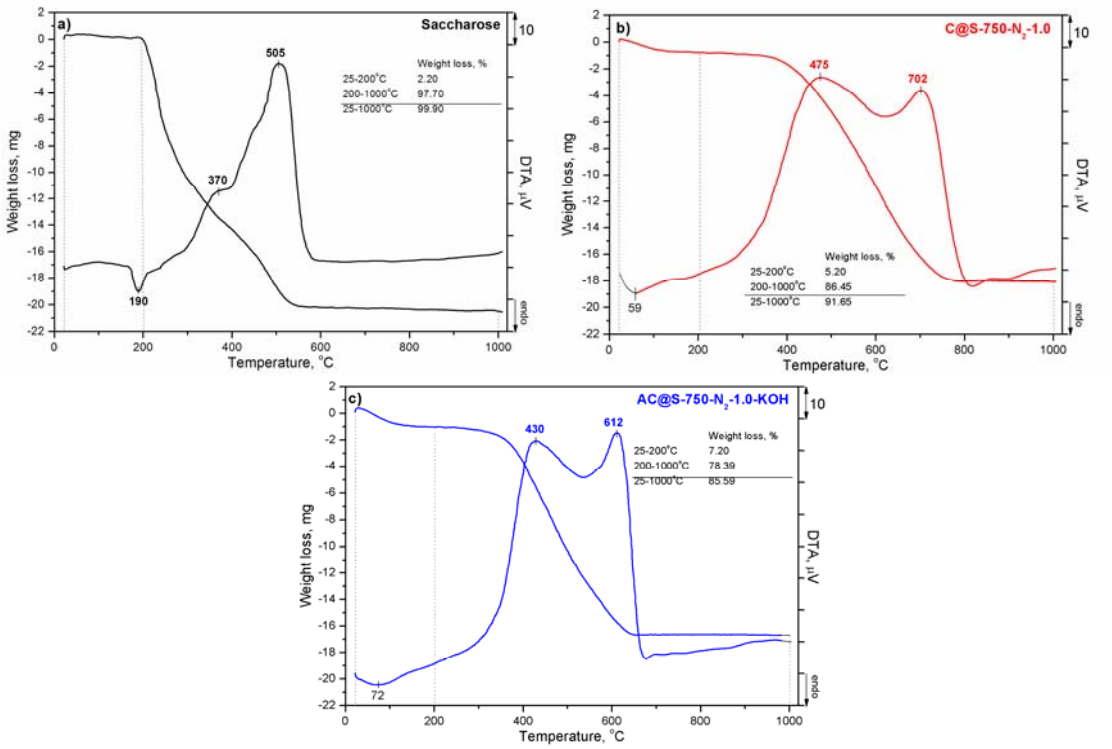

Fig. 8. Thermal analysis of: a) saccharose; b) C@S–750–N_2–1.0 and c) AC@S–750–N_2–1.0–KOH.

It is clear from Fig. 8c it is clear that after activation of the C@S–750–N_2–1.0 the shape of the TGA and DTA curves did not change significantly. Also, all DTA peaks characteristic for C@S–750–N_2–1.0 were visible on the DTA curve of the activated sample. However, due to activation, the endothermic DTA peak characteristic for moisture loss is shifted towards higher temperatures and it was observed at 72 °C. Also, for AC@S–750–N_2–1.0–KOH in the first temperature region (25–200 °C) a slightly higher weight loss was observed by TG analysis (7.20 %). On the other side, exothermic DTA peaks characteristic for decomposition of organic components were shifted to lower temperatures and were observed at 430 and 612 °C. This process was followed with lower mass loss in the TGA diagram in comparison with C@S–750–N_2–1.0 which was finished at about 650 °C. Further increase of temperature did not lead to significant changes in the TGA curve and total weight loss in the 200–1000 °C interval was about 78 %. Finally, it may be concluded that shifting of the endothermic DTA peak to higher temperature and higher mass loss obtained by TG analysis in the first temperature region for activated sample, indicates increase of the hydrophilicity of the surface of the activated sample in comparison with C@S–750–N_2–1.0. On the other side, shifting of exothermic DTA peaks characteristic for decomposition of the organic components to lower temperatures and lower mass loss obtained in the second temperature interval (200–1000 °C) may be an indication that activation process has a negative effect on the thermal stability of the sample. Actually, during activation with KOH

fraction of organic components were probably decomposed or removed by dissolution, and consequently lower energy (temperature) is required for thermal decomposition.

The exothermicity observed for both samples means that the energy released from their thermal treatment was higher than the energy absorbed for bond scission, oxidation, decomposition, burning, *etc*. There is a possibility to collect the energy produced from the decomposition of these materials. Kinetic analysis is important for better understanding of the thermal degradation reactions of the materials. To examine whether these materials have the potential to be used as a source of energy, their thermal kinetic analysis was studied. From that reason both samples were thermally treated with different heating rates (from 5 to 20 °C), and results of derivative thermogravimetric analysis (DTG) were used to determine all necessary parameters. Obtained results are given in Fig. 9a and 9b.

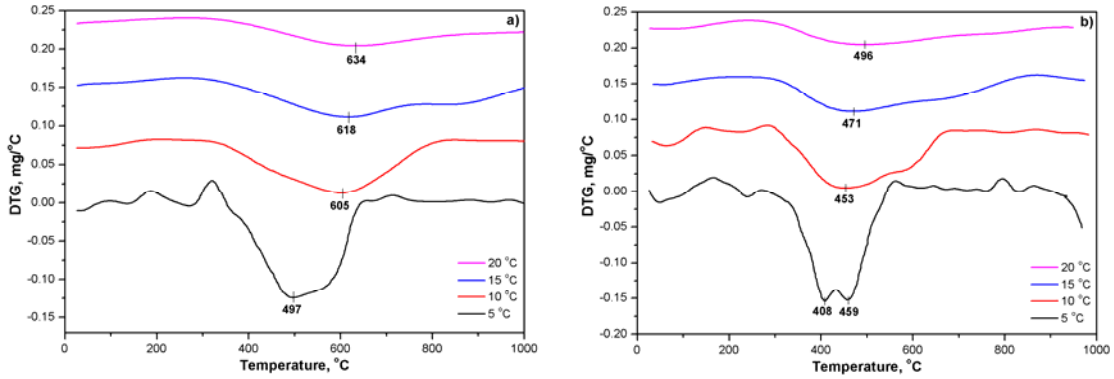

Fig. 9. Influence of heating rate on the DTG curve of: a) C@S–750–N_2–1.0 and b) AC@S–750–N_2–1.0–KOH.

Fig. 9. shows DTG curves of the C@S–750–N_2–1.0 and AC@S–750–N_2–1.0–KOH at several heating rates. It was found that for both samples, by increasing the heating rate the decomposition temperature of the organic components, was shifted to higher temperatures. For further kinetic investigations and calculations of the kinetic parameters, only the highest exothermic peaks at 497 °C for C@S–750–N_2–1.0, and 408 °C for AC@S–750–N_2–1.0–KOH were used (Fig. 8b and 8c). Kissinger's method [46] was used to determine kinetic parameters such as pre-exponential factor (A) and activation energy (E_a). To calculate the pre-exponential factor (A), according to Arrhenius equation, it was assumed that the decomposition of organic constituents followed first order kinetics. Applying this method curves $\ln(\beta/T_p^2)=f(1/T_p)$ were plotted for both samples and results are shown in Fig. 10.

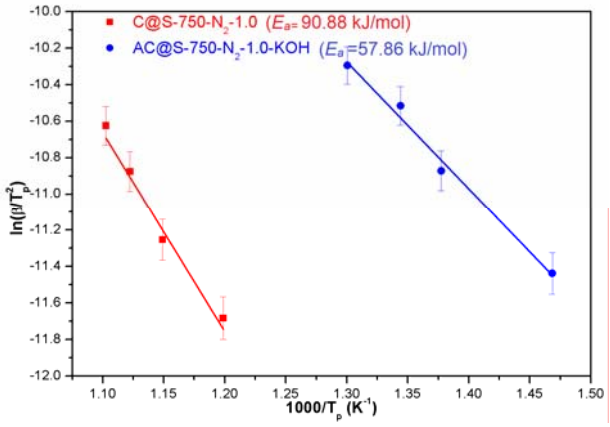

Fig. 10. Plot of $\ln(\beta/T_p^2)$ versus reciprocal peak temperature $1/T_p$for C@S–750–N_2–1.0and AC@S–750–N_2–1.0–KOH.

As it may be seen from Fig. 10. curve $ln(\beta/T_p^2)$ versus $1/T_p$ showed linear trends (r^2>0.95) for both samples indicating that first-order kinetics provides a good description of the overall observed decomposition behaviour in this temperature range [47]. The activation energies (E_a) for both samples were calculated from the slope of the curves which is equal to $-E_a/R$, R is molar gas constant (8.314 J/K mol), while pre-exponential factor, lnA was calculated from equation 1 [48].

$$A = \beta\left(\frac{E_a}{RT_p^2}\right)\exp\left(\frac{E_a}{RT_p}\right) \quad (2)$$

Thermodynamic parameters, Gibbs free energy (ΔG), enthalpy (ΔH) and entropy (ΔS) were calculated based on the kinetic parameters (A and E_a) from the following equations [49].

$$A\exp\left(\frac{-E_a}{RT}\right) = \upsilon\exp\left(\frac{-\Delta G}{RT}\right) \quad (3)$$

$$\Delta H = E_a - RT \quad (4)$$

$$\Delta G = \Delta H - T\Delta S \quad (5)$$

Where $\upsilon=k_BT/h$, where k_B and h are Boltzmann and Plank constants, respectively, T is temperature of peak (K). Corresponding results are given in Tab.s III and IV.

Tab. III Calculated pre-exponential factors.

C@S–750–N_2–1.0			AC@S–750–N_2–1.0–KOH		
β (K/min)	T_p, ^oC (K)	ln (A) (min^{-1})	β (K/min)	T_p, ^oC (K)	ln (A) (min^{-1})
5	497 (770)	11.79	5	408 (681)	7.63
10	605 (878)	12.97	10	453 (726)	7.55
15	618 (891)	10.71	15	471 (744)	7.72
20	634 (907)	10.70	20	496 (769)	7.62
Average		11.54	Average		7.63

Tab. IV Calculated thermodynamic parameters.

	E_a (kJ/mol)	ΔG (kJ/mol)*	ΔH (kJ/mol)*	**ΔS** (J/mol K)*
C@S–750–N_2–1.0	90.88	259.34	83.58	-199.87
AC@S–750–N_2–1.0–KOH	57.86	161.89	51.82	-151.61

*For peaks observed at temperature rate of 10 ^{o}C/min.

As can be seen from Tab. IV the activation energy required for thermal degradation of carbonated sample decreased after its activation with KOH and the E_a value decreased from 90.88 kJ/mol for C@S–750–N_2–1.0 to 57.86 kJ/mol for AC@S–750–N_2–1.0–KOH. Positive values of the Gibbs free energies (~259 and ~162 kJ/mol for C@S–750–N_2–1.0 and AC@S-750-N_2-1.0-KOH, respectively) obtained for both samples confirm that decomposition of organic constituents is not spontaneous. At the same time, positive values of the entropy (~84 and ~52 kJ/mol for C@S–750–N_2–1.0 and AC@S–750–N_2–1.0–KOH, respectively) confirm that process of decomposition of organic constituents is not possible without addition of the external energy. It is important to notice that, for activated sample, all three parameters (E_a, ΔG and ΔH) are lower than for C@S–750–N_2–1.0 which means that activation with KOH may cause the decrease of the materials processing temperature decrease and possibly allows

lowering of the thermal treatment cost [50]. Calculated E_a in this study are much lower in comparison with those obtained in the literature for different materials such as fibers (E_a ~160-170 kJ/mol) [51], wood species (E_a~180-210 kJ/mol) [52] or for different polymers (E_a~240 kJ/mol) [53]. From this point, it may be concluded that both samples, especially sample activated with KOH, have a potential to be used for energy production. This is additionally supported with fact that for both samples only 10–15 % of the waste remains after thermal degradation process. Also, the existence of exothermal DTA peaks (Fig. 6.) means that a higher amount of energy is released than energy necessary to start the degradation process.

3.7. Adsorption studies

The examination of alkali activated carbon materials, as potential adsorbents, for removal of MO and MB were performed. The adsorption measurements were carried out with same concentrations of the dye solutions (50 mg/dm^3). The absorption spectra of dye solutions were collected after certain time intervals and at the certain absorption wavelength, λ_{max}= 665 nm for MB, and λ_{max}=466 nm for MO, as well. As it can be seen from absorptions spectrum (Fig. 11. and Fig. 12.), the characteristics bands decreased significantly for samples activated with NaOH and KOH, indicating that MB and MO were removed from the solution. It may be noticed that solutions were almost colorless after 5 min, which is not case for sample activated with LiOH.

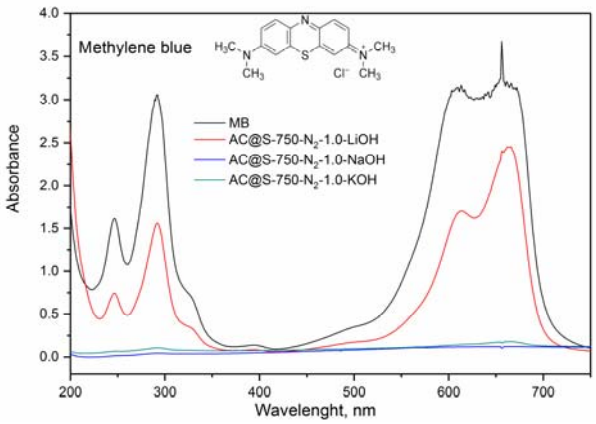

Fig. 11. Absorption spectra of the MB dye solutions (50 mg/dm^3) before and after introducing alkali activated carbon powder. Solid/liquid ratio: 25 mg/25 cm^3.

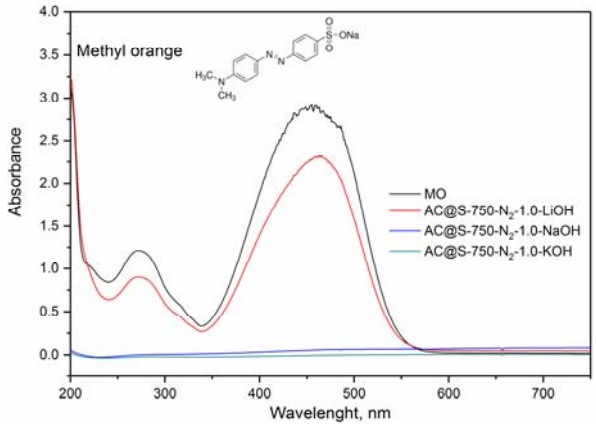

Fig. 12. Absorption spectra of the MO dye solutions (50 mg/dm^3) before and after introducing alkali activated carbon powder. Solid/liquid ratio: 25 mg/25 cm^3.

The sample activated with LiOH showed different behavior depending on dye solution. In the case of MB, samples activated with LiOH, achieved equilibrium after 80 min (Fig. 13.). On the other hand, in the case of MO, the LIOH activated sample showed poorer adsorbent quality and equilibrium state has not been achieved even after 5 h (Fig. 14.). However, for KOH and NaOH activated samples, the equilibrium states were achieved after 20 min (Fig. 13. and Fig. 14.).

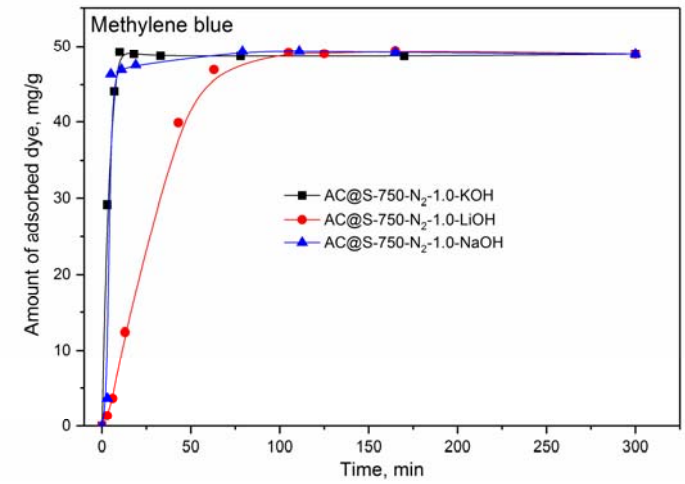

Fig. 13. Amount of adsorbed MB for ACs activated with three alkalis (●LiOH, ▲NaOH and ■ KOH). C_i(MB)= 50 mg/dm^3. Solid/liquid ratio: 25 mg/25 cm^3.

The adsorbed amounts of dyes were determined by using mass balance relationship:

$$q_e = (C_o - C_e)\ V/m \quad (6)$$

where q_e represents the amount of dye adsorbed per unit mass of adsorbent (mg/g), C_0 is initial concentration of dyes (mg/dm^3), while C_e is the equilibrium liquid phase concentration of dyes (mg/dm^3), V is the volume of the solution (dm^3), and m is the mass (g) of sample [54, 55].

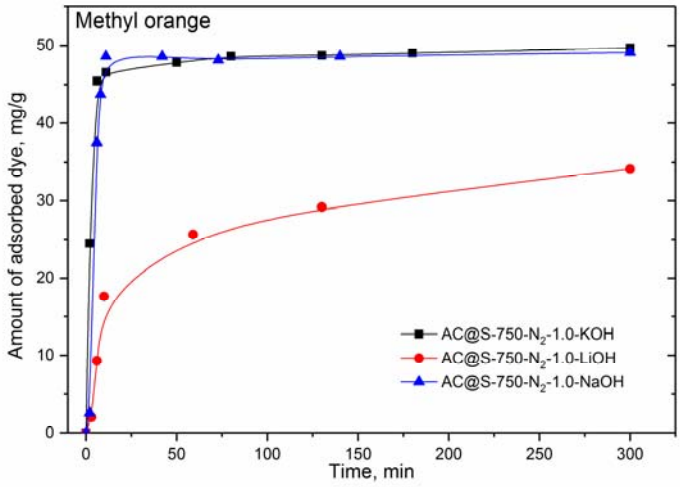

Fig. 14. Amount of adsorbed MO for ACs activated with three alkalis (●LiOH, ▲NaOH and ■ KOH). C_i(MB)= 50 mg/dm^3.Solid/liquid ratio: 25 mg/25 cm^3.

The dependences of the amounts of adsorbed dyes from contact time are illustrated in Fig. 13. for MB and in Fig. 14. for MO, respectively, for all three alkali activated carbon samples. As it may be seen from Fig. 13. and Fig. 14., for all three curves, it is characteristic that the adsorption process is rapid in the initial stage, for both dyes MB and MO. In the later stage, adsorption process becomes much slower. As already mentioned, the KOH and NaOH activated carbon samples achieved equilibrium after 20 min and practically curves overlapped after this time (Fig. 13. and Fig. 14.).

The adsorption rate for KOH and NaOH carbon activated samples was much higher at the beginning for both, MB and MO dyes. In general, better elimination of MB and MO for KOH and NaOH activated carbon samples was observed in initial stage of adsorption process, whereas the adsorption rate of MO and particular MB was significantly lower for LiOH activated samples in initial stage of process. Furthermore, for LiOH activated carbon samples equilibrium state for MO has not been achieved even after 5 h. After reaction time, all three alkali activated carbon samples in the case of MB removed ~50 mg/g. For the MO, NaOH and KaOH activated samples removed about 50 mg/g, while LiOH activated sample removed significantly lower amount of the MO (~35 mg/g).

4. Conclusion

Obtained results showed that differences in morphology between carbon microspheres obtained by hydrothermal treatment of saccharose with two different concentrations (HTC@S–240–0.5–24 and HTC@S–240–1.0–24) can be observed only at 240 °C where the presence of interconnected microspheres with incompletely developed spherical shape is clearly visible. The carbon microspheres treated with NaOH and KOH and then carbonized at 750 °C in nitrogen flow changed their spherical shape and became disordered but possess significant increase of the specific surface area. The highest specific area was measured for sample activated with KOH (2245 m^2/g). Contrary to that, carbon microspheres treated with LiOH as activated agent, and carbonized at 750 °C in nitrogen flow, maintained their microspherical structure but, even increasing of the specific surface was noted (from lower than 10 to ~320 m^2/g) the increase was much lower in comparison with carbons activated with KOH and NaOH.

Results of the elemental analysis showed that sample obtained by HTC treatment at 240 ^oC and for saccharose concentration of 1 mol/dm^3 possess the best properties i.e. the content of carbon (~70 % and yield ~25 %). Further carbonization increased the content of carbon in carbon microspheres up to ~85 % AC@S–750–N_2–1.0–NaOH and AC@S–750–N_2–1.0–KOH while the content of carbon in activated carbon AC@S–750–N_2–1.0–LiOH significantly decreased to only 36.6 %.

Results of the XRPD analysis illustrated that samples of active carbons AC@S–750–N_2–1.0–NaOH and AC@S–750–N_2–1.0–KOH were mainly in an amorphous state, while in contrast to these results, XRPD pattern of sample AC@S–750–N_2–1.0–LiOH shows sharp and well-defined peaks indicating that this material possess besides amorphous, a defined structural arrangement.

The results of the FTIR analysis showed that there are no significant differences in structural properties.

Results of thermal analysis (TGA/DTA) and thermal degradation kinetic indicate that AC@S–750–N_2–1.0–KOH has a potential to be used for energy production (E_a ~ 58 kJ/mol), which was additionally supported with fact that after thermal degradation process remain only 10–15 % of waste.

Adsorption experiments showed that activated carbons synthesized by activation with KOH and NaOH possess good properties for MO and MB removal from

contaminated water solutions, while LiOH activated sample showed good adsorption only for MB.

Acknowledgements

The financial support of this research work was provided by the Ministry of Education and Science of the Republic of Serbia, projects III45005 and III45012 and TR34013.

5. References

1. A. Matilainen, M. Vieno, T. Tuhkanen, Environ. Int., 32 (2006) 324.
2. J. Guo, A. C. Lua, Chem. Eng. Res. Des., 81 (2003) 585.
3. Y. Liu, Z. Shen, Carbon, 43 (2005) 1574.
4. P. Serp, P. M. Corrais, P. Kalck, Appl. Catal., A 253 (2003) 337.
5. J. B. Joo, Y. J. Kim, W. Kim, P. Kim, J. Yi Catal. Commun., 10 (2008) 267–271.
6. P. G. Collins, A. Zettl, H. Bando, A. Thess, R. E. Smalley, Nanotube nanoevice. Science., 278 (1997) 100.
7. M. Isao, K. Cha-Hun, K. Yozo, Carbon, 39 (2001) 399.
8. M. Endo, C. Kim, K. Nishimura, T. Fujimo, K. Miyashita, Carbon, 38 (2000) 183.
9. N. Venkatesan, J. Yoshimitsu, Y. Ito, N. Shibata, K. Takada, Biomaterials, 26 (2005) 7154.
10. H. Zhu, M. J. Mc Shane, J. Am.Chem.Soc., 127 (2005) 13448.
11. M. B. Shiflett, H. C. Foley, Science, 285 (1999) 1902.
12. T. Kyotani, Carbon, 38 (2000) 269.
13. A. P. Parra, M. Vlasova, P. A. M. Aguilar, T. Tomila, Sci. Sinter, 49 (2017) 207.
14. B. Crittenden, A. Patton, C. Jouin, S.Perera, S.Tennison, J. A. Echevarria, Adsorption, 11 (2005) 537.
15. C. Brasquet, P. Le Cloirec, Carbon, 35 (1997) 1307.
16. E. Yasuda, M. Inagaki, K. Kaneko, M. Endo, A. Oya, Y. Tanabe, Carbon alloys: Novel concepts to develop carbon science and technology. Oxford: Elsevier Science, 2003. (in English)
17. R. C. Bansal, J. B. Donet, F. Stoeckli, Active carbon. Marcel Dekker, New York, 1988. (in English)
18. Q. Wang, X. Y. Liang, R. Zhang ,C. J. Liu, X. J. Liu,W. M.Qiao, L. Zhan, L. Ling, New Carbon Mater., 24 (2009) 55.
19. B. Hu, K. Wang, L. Wu, S. H. Yu, M. Antonietti, M. Titirici, Adv. Mater., 22 (2010) 813.
20. A. Maklad, A. Emara, E. El-Maddah, M-A. El-Refai, J. App. Pharm. Sci., 2 (2012) 1.
21. M. Sevilla, A. B. Fuertes, Chem. Eur. J., 15 (2009) 4195.
22. A. Romero-Anaya, M. Ouzzine, M. Lillo-Rodenas, A. Linares-Solano, Carbon, 68 (2014) 296.
23. Q. Wang, H. LI, L. Chen, X. Huang, Solid State Ion., 43 (2002) 152.
24. N. Jović-Jovičić, P. Banković, Z. Mojović, B. Nedić-Vasiljević, S. Marinović, T. Mudrinić, A. Milutinović-Nikolić, Sci. Sinter., 49 (2017) 419.
25. B. Hameed, A. Din, A. Ahmad, J. Hazard. Mater., 141 (2007) 819.
26. M. Rafatullah, O. Sulaiman, R. Hashim, A. Ahmad, J. Hazard. Mater., 177 (2010) 70.
27. A. Mittal, A. Malviya, D. Kaur, J. Mittal, L. Kurup, J. Hazard. Mater. 148 (2007) 229.

28. J. Yi, L. Zhang, Bioresour. Technol., 99 (2008) 2182.
29. X. Luo, L. Jhang, J. Hazard. Mater., 171 (2009) 340.
30. E. Haque, J. Jun, S.Jhung, J. Hazard. Mater., 185 (2011) 507.
31. Powder Diffraction File, PDF-2 Database, announcement of new data- base release 2012, International Centre for Diffraction Data (ICDD).
32. E. Barrett, L. Joyner, P. Halenda, J. Am. Chem. Soc., 73 (1951) 373.
33. K. Kaneko, C. Ishii, H. Kanoh, Y. Hanzawa, N. Setoyama, T. Suzuki, Adv. Colloid Interface Sci., 76–77 (1998) 295.
34. W. H. Weber, K. C. Hass, J. R. Mcbride, Phys. Rev. B. 48 (1993) 178.
35. S. Tsunekawa, J. –T. Wang, Y. Kawazoe, J. Alloy. Compd. 408–412 (2006) 1145.
36. K. S. W. Sing, D. H. Everett, R. A.W. Haul, L. Moscou, R. A. Pierotti, J. Rouquerol, T. Siemieniewska, Pure Appl. Chem. 57 (1985) 603.
37. A. Omri , M. Benzina, Journal de la Société Chimique de Tunisie, 14 (2012) 175.
38. C. H. Yao, Y.S. Shin, L. Q. Wang, C. F. Windish, W. D. Samuels, B. W. Arey, C.M. Wang, J. Phys. Chem. C., 111 (2007) 15141.
39. M. J. A. Antal, W. S. L. Mok, Carbohydr. Res. 199 (1990) 91.
40. S. P. Verevkin, V. N. Emelyanenko, E. N. Stepurko, R. V. Ralys, D. H. Zaitsau, A. Stark, Ind.Eng.Chem. Res. 48 (2009) 10087.
41. N. Baccile, G. Laurent, F. Babonneau, F. Fayon, M. Titirici, M. Antonietti, J .Phys. Chem. C. 113 (2009) 9544.
42. C. Sellitti,J. L. Koenig, H. Ishida, Carbon, 28 (1990) 221.
43. E. Fuente, J. A. Menéndez, M. A. Díez, D. Suárez, M. A. Montes-Morán, J. Phys. Chem. B. 107 (2003) 6350
44. N. Djordjevic, S. Martinovic, M. Vlahovic, P. Jovanic, V. Vidojkovic, T. Boljanac, Sci. Sinter. 41 (2009) 267.
45. S. L. Iconaru, F. Ungureanu, A. Costescu, M. Costache, A. Dinischiotu, D. Predoi, J.Nanomater. 2011 (2011) 1.
46. I. F. Myronyuk, V. I. Mandzyuk, V. M. Sachko, V.M. Gunko, Nanoscale Res. Lett. 11 (2016) 508.
47. H. E. Kissinger, J. Res. Nat.Bur. Standards, 57 (1956) 217.
48. M. Sunitha, C. P. Reghunadhan Nair, K. Krishnan, K. N. Ninan, Thermochim. Acta. 374 (2001) 159.
49. M. R. Sovizi, S. S. Hajimirsadeghi, B. Naderizadeh, J. Hazard. Mater. 168 (2009) 1134.
50. M. Šumar Ristović, D. Minić, V. Blagojević, K. Anđelković, Sci. Sinter. 46 (2014) 37.
51. H. Zhen, Y. Xiaoxu, P. Xi, Z. Yulong, F. Meifen, Z. Qiang, Proceedings of the 17th IAPRI world conference on Packing, Tianjin, China, (2010) 406.
52. F. Yao, Q. Wu, Y. Lei, W. Guo, Y. Xu, Poly. Degrad. Stab. 93 (2008) 90.
53. M. Poletto, A. Zattera, R. Santana, Bioresour. Technol. 126 (2012) 7.
54. L. Abate, I. Blanco, A. Pollicino, A. Recca, J. Therm. Anal. Calorim. 70 (2002) 63.
55. J. W. Lee, S. P.Choi, R. Thiruvenkatachari, W. G. Shim, H. Moon, Dyes Pigm. 69 (2006) 196.
56. N. Tomić, Z. Dohčević-Mitrović, N. Paunović, D. Mijin, N. Radić, B. Grbić, S. Aškrabić, B. Babić, D. Bajuk-Bogdanović, Langumir, 30 (2014) 11582.

Садржај: *У представљеном раду испитани су утицај температуре, концентрације полазног материјала и различитих хидроксида на својства активираних угљеничних материјала добијених из сахарозе. Узорци су припремљени хидротермалним третманом и активирани помоћу KOH, NaOH и LiOH. Две различите концентрације воденог раствора сахарозе (0,5 1,0 mol/dm^3) и три температуре (160, 200, 240 ºC) су*

примењене у хидротермалном третману. Процеси активације су изведени на 750 ºC у атмосфери азота. Узорци су карактерисани рендгендском дифрактометријском анализом, елементарном анализом, адсорпционо-десорпционим мерењем азота, инфрацрвеном спектрометријом са Фуријеовом трансформацијом, скенирајућом електронском микроскопијом и термијском анализом. Добијени узорци су такође тестирани за потенцијалну примену у уклањању боја из водених раствора.
Кључне речи: *сахароза, активни угаљ, хидротермални третман, извори енергије.*